Future Technology
Open Access Journal
ISSN 2832-0379

May 2023| Volume 02 | Issue 02 | Pages 36-42

Journal homepage: https://fupubco.com/futech

https://doi.org/10.55670/fpll.futech.2.2.5

Future Publishing LLC

Article

Next generation of advanced ceramic 3D printers

Sam Choppala*, Armin Allam, Zichen Fang, Amir Armani

San Jose State University, California, United States of America

ARTICLE INFO

Article history:
Received 08 November 2022
Received in revised form
09 December 2022
Accepted 13 December 2022

Keywords:
Additive manufacturing, Technical ceramics
3D Printing, Extrusion, Machine learning

*Corresponding author
Email address: sam.choppala@sjsu.edu

DOI: 10.55670/fpll.futech.2.2.5

ABSTRACT

Ceramic on-demand extrusion (CODE) is a novel slurry-based additive manufacturing (AM) process for technical ceramics. Extensive characterization studies have shown that this process produces dense ceramic specimens with relatively improved mechanical properties such as flexural strength, fracture toughness, hardness, etc. The objective of the current study was to develop the next generation of CODE. The CODE printer created consists of an aluminum extrusion frame, a three-axis gantry system, an extruder, and a heat lamp. The ceramic slurry is fed to an extruder that prints parts onto a bedplate. The green body parts are then subject to postprocessing, including drying, debinding, and sintering. Ceramic composites and functionally graded materials are created using CODE to further study the process. Furthermore, a real-time deep learning defect detection protocol to identify common defects of CODE while printing, as well as a control feedback system to implement corrective action based on the defect detected, is being developed.

1. Introduction

Technical ceramics are versatile materials used in various industries and applications due to their hardness, stability at high temperatures, chemical resistance, electrical insulation, and more. Examples of common technical ceramic materials include various types of oxides, carbides, nitrides, and borides. A few examples of present-day applications include zirconia-based dental abutments and implants [1], calcium phosphate-based synthetic bone grafts [2], and silicate-based high-frequency dielectrics for high-bandwidth wireless communications [3]. As the use of technical ceramics is prevalent in today's applications, the quality, efficiency, and speed of manufacturing these components are crucial. Under ceramic manufacturing, there are two main distinct types of processes: conventional fabrication and additive manufacturing. Another subcategory within conventional fabrication includes pressure-less sintering methods and high-pressure sintering methods. This subcategory distinguishes the conventional fabrication methods by the application of external pressure while sintering to densify the component further. Examples of conventional fabrication methods include gel casting [4], direct foaming [5], isostatic pressing [6], slip casting [7], etc. AM methods could perform better in creating ceramic components with complex geometries and designs [8]. Examples of AM processes include stereolithography [9], direct ink writing [10], binder jetting [11], and selective laser sintering [12]. These processes can be classified based on the type of feedstock used, which can be either powder-based or slurry-based. Further detailed information regarding ceramic AM techniques can be found in [13-15]. Ceramic on-demand extrusion (CODE) is a novel slurry-based 3D printing technology used to create ceramic components. The main procedure includes a green body that is printed in a layer-wise fashion [16]. After each layer is printed, a heat lamp is used to dry the printed layer partially and uniformly. Then, layers below the last layer will submerge into an oil bath to prevent evaporation from the sides of the part and preserve moisture. This process will occur sequentially until the green body is completely printed. This paper outlines and discusses the CODE, the current progress of the process, as well as the artificial intelligence implementation procedure to improve ceramic 3D printing with CODE.

2. Printer Design

2.1 Mechanical Design

The main structure of the CODE 3D printer includes aluminum extrusions, rails (X, Y, and Z), an extruder, an oil bath, a heat lamp, servo motor drivers, and a printing build plate displayed in Figure 1. The frame was built by twelve 80 mm × 80 mm aluminum T-slot extrusions (40-8080, 80/20 LLC, Columbia City, IN) and four 40 mm × 80 mm aluminum T-slot extrusions. The extrusions are connected by twelve L-brackets and several T-nuts. The 4080 extrusions and L-brackets enhance the strength and stability of the 3D printer. There are three rails with actuators used in this printer. The X and Y rails utilize the same 100 W servo motors (MINAS A6 100W Servo Motor, Panasonic, Osaka, Japan); the Z rail also has a 100W servo motor but with an independent brake attached. To make the Z rail fully functional, it is necessary to have an external power supply to power the brake so that it can be released.

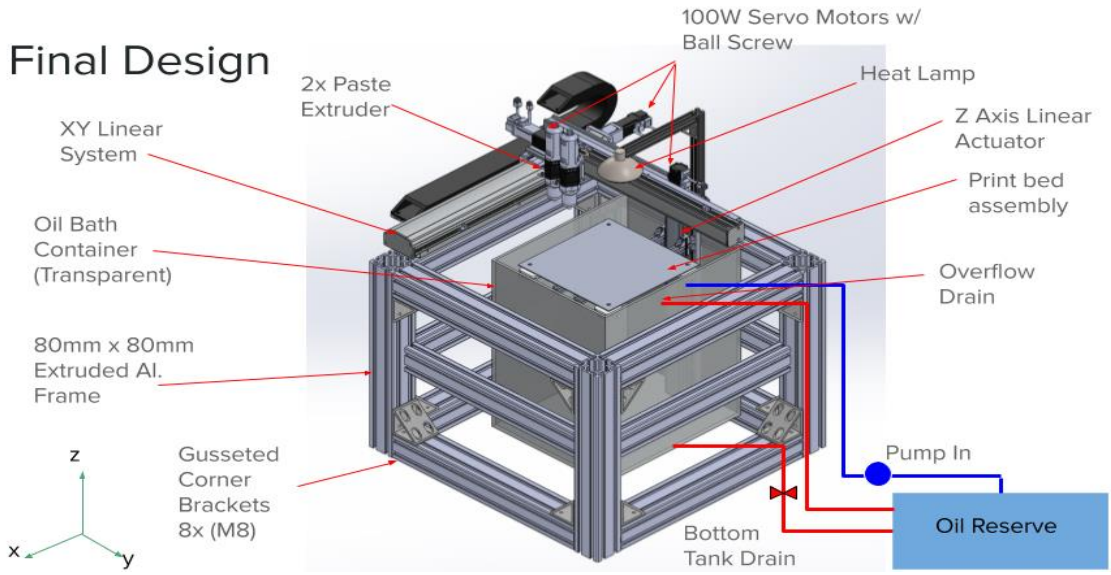

Figure 1. Annotated 3D model of a prototype design for the CODE method

Three Panasonic drivers were purchased along with X, Y, and Z rails to control the motors in the rails. As displayed in Figure 2, the heat lamp is mounted onto the frame, utilizing a custom 3D-printed mounting adapter. After the printer prints each layer, the heat lamp will turn on automatically, using the G code to dry the printed layer. Once a layer is printed, the extruder returns to the home position, triggering the heat lamp to turn on and partially dry the printed layer. After each layer is printed and dried, the printing bed attached to the Z (i.e., vertical) rail will move down to merge the newly finished layer into the oil tank.

2.2 Electrical Design

The code printer user can insert G code into the LinuxCNC software to generate motion signals. Linux CNC is an open-source CNC software that is commonly used to operate milling machines, laser cutters, lathes, and more. These signals are output to the MESA 7i76 (MESA Electronics, 7i76, El Sobrante, CA) daughter board from the MESA 6i25 (MESA Electronics, 6i25, El Sobrante, CA) board in the motherboard of the host computer. To operate the Panasonic motors (Panasonic, Minas A6, Osaka, Japan) that drive the linear rails in the X, Y, and Z directions, they must be paired with MINAS A6 Panasonic drivers. The MESA 7i76 output sends step and direction signals to the drivers through the X4 I/O port on the Panasonic drivers (Panasonic, Minas A6 Osaka, Japan). 5VDC power is administered to the MESA 7i76 board from the computer power supply. The MESA 7i76 board receives power from two external sources. One from a pin out of the IEEE 1284 36-pin male (i.e., DB25) cable connected to the MESA 7i76 board coming from the MESA 6i25 board and another 12VDC from an external power supply to power the board and field power outputs, respectively. The drivers are powered by external AC power, and feed power to the servo motors. A flowchart diagram displaying the power and communication lines between the electrical components of this system is shown in Figure 3.

Figure 2. Prototype CODE Printer

2.3 Hardware-Software Implementation

To control the physical hardware system, the LinuxCNC operating system is used, along with two different MESA boards and a microstep driver. The two MESA boards being used are MESA 6i25 and MESA 7i76. The MESA 6i25 board is a general-purpose programmable I/O card for the PCIe bus of a computer. This board is directly connected to the host computer's motherboard using the PCIe x1 port.

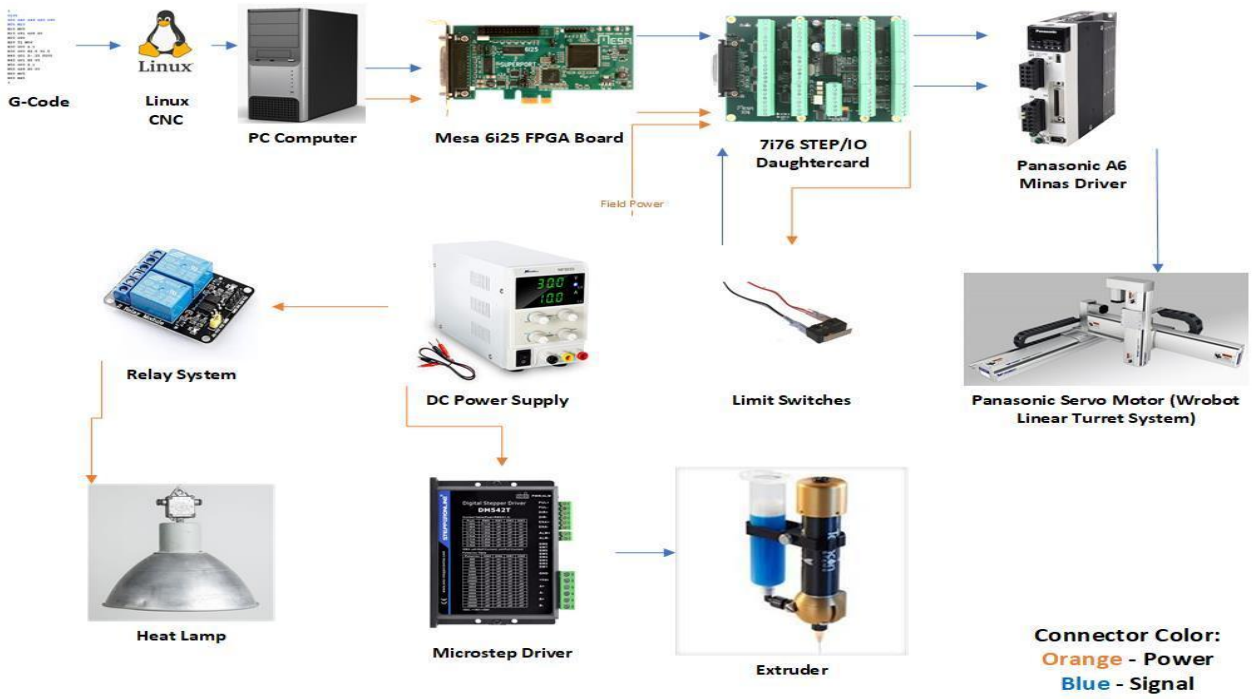

Figure 3. CODE printer process diagram

Furthermore, the MESA 7i76 is classified as a daughter board, meaning it connects to and communicates with the MESA 6i25, instead of the host computer directly. The MESA 7i76 connects to the MESA 6i25 using a DB25 cable, as discussed in Section 2.2. The MESA 7i76 board is used for interfacing with the drivers of the motor directly using step and direction interfaces. It sends digital step pulses to control the motor drivers. A microstep driver is used to control the extruder, as it is a stepper motor. The hardware can be controlled by G code thru the LinuxCNC software interface. The top row of Figure 3 displays the signal flow from the LinuxCNC software to the MESA 7i76, where the drivers obtain the final communication signal to operate the motors. The main method of controlling the motors with the MESA boards is through LinuxCNC being installed onto the host computer. The host computer is selected such that the desktop latency, when measured with LinuxCNC is as low as possible. The host computer has a desktop latency of around 9000 ns. Within LinuxCNC, the PNC configuration wizard is used to set up the connections between the motor drivers and the MESA boards, as well as the models of the boards being used and their firmware. The setup of the PNC configuration results in two files with the following extensions: .hal and .ini. These files can be used to set up PID gains, servo period, and other variables. The LinuxCNC interface relies on the information from the .hal and .ini files to communicate with the operating system and the MESA boards.

3. Preprocessing

CODE is a slurry-based extrusion process, and the feedstock is in the form of a viscous paste. The four main materials used in this slurry are as follows: deionized water, ceramic powder, dispersant, and binder. Within the slurry, water and ceramic powder cover the majority of the final volume. Additional modifications can be made to the paste by adding or removing certain materials for different printing applications.

The amount and ratio of each material in the slurry are dependent on the solids loading and the paste viscosity desired. The dispersant in the mixture is used to create a homogeneous slurry. The purpose of this is such that the ceramic particles do not settle at the bottom over time. The use of a dispersant allows for more homogenous green bodies when printed. The binder is used to both thicken the paste and act as a bonding agent within the green bodies when printed. The amount of binder is the least with respect to volume out of all the materials used within the slurry. The preprocessing phase for any CODE printing material would involve the same major stages. The general outline is shown below. This outline is visually displayed in Figure 4.

- **Step 1.** Combine water, dispersant, and ceramic powder.
- **Step 2.** Mix in a ball mill with appropriate ceramic milling media for uniform paste in a closed container. The time depends on the volume of paste, solids loading, size of ball mill ceramic beads, and ceramic powder particle size and distribution or until the paste is homogenous.
- **Step 3.** Add binder after ball milling the mixture.
- **Step 4.** Use a vacuum whip mixer to mix the binder into the paste uniformly. The time depends on the volume of paste and amount of binder or until the paste is homogeneous.
- **Step 5.** Use a vibratory table to set the paste (i.e., eliminate remaining air bubbles)

4. Processing

After creating the feedstock, the material is transferred into a hopper system that feeds the feedstock into the extruder. The extruder is then moved in the X and Y directions to complete the first layer of the print using Luer-lock tips for precise control of the slurry. After the first layer is completed, the heat lamp is turned on until the printed layer is partially dried. This stage is followed by the Z-axis moving down such that the partially dried layer is submerged in an oil bath. The printer then repeats these stages and prints in a layer-wise fashion while each layer is appropriately partially dried and

submerged in an oil bath. After all the layers are printed, the printed specimen will be submerged in the same oil bath for a certain time duration such that significant gradients in mechanical properties and specimen surface qualities are avoided. The G code used for this printer follows the standard, which is supported by LinuxCNC. The heat lamp is treated the same as the coolant such that it is controlled by LinuxCNC using the same M code as the coolant function within LinuxCNC, as the coolant is not needed for this printer. Furthermore, the extruder is treated as a fourth axis such that the dosing and extrusion speed is properly controlled with the G code. Processing parameters for printing specimens include extrusion rate, nozzle diameter, extruder movement speed, layer thickness, line spacing, heat lamp height, and lamp timing. These variables are all interconnected and are determined empirically for various printing applications.

5. Postprocessing

The postprocessing phase involves three main stages. These stages are visually displayed as a flowchart in Figure 5.

- **Step 1.** Send printed green bodies to a humidity chamber to dry the green bodies of water. The time depends on the solids loading of the paste and the size of the printed specimens, and typically takes less than a day.
- **Step 2.** Use a furnace to debind the dried specimens. The time depends on the amount of binder used and the size of the printed specimens, and typically takes less than two hours.
- **Step 3.** Use a sintering furnace to densify the parts. The time and heating rate depend on the material composition, particle size, sintering aids, and green body density. It typically takes a few hours.

The debinding stage (Step 2) and the sintering stage (Step 3) both use the sintering furnace; however, the sintering schedule (i.e., sintering time, sintering temperature, and heating rate) are different. The debinding stage will be done at a much lower temperature and for a shorter time than the sintering stage, as the binder will burn out in a shorter time than the full densification of the ceramic specimen. Ghazanfari et al. [16,18,19] delve into further specific examples of materials, pre-processing, and postprocessing parameters.

6. Sample Parts

Some sample parts printed using CODE are shown in Figure 6. Samples (a), (b), (c) in figure 6 are comprised of zirconia powder (TZ-3Y-E, Tosoh USA, Inc., Grove City, OH, USA) as the main ceramic material, Dolapix (Dolapix CE 64, Zschimmer & Schwarz GmbH, Lahnstein, Germany) as a dispersant, ammonium hydroxide solution (221228, Sigma Aldrich, St. Louis, MO, USA) for pH adjustment, and deionized water. Sample (d) in figure 6 is comprised of alumina powder (A-16SG; Almatis, Leetsdale, PA) as the main ceramic material, ammonium polymethacrylate (DARVAN® C-N; Vanderbilt Minerals, Norwalk, CT) as a dispersant, cold-water-dispersible methylcellulose (Methocel J5M S; Dow Chemical Company, Midland, MI) as a binder, and deionized water. A similar pre-processing procedure, as described in Section 3, was used to prepare the final slurry with 60 vol% solids loading for the alumina samples and 50 vol% solids loading for the zirconia samples. Figure 6 below displays the sample test specimens with varying geometric complexities produced with this slurry. The printing parameters used to create the zirconia samples used a nozzle diameter of 600 µm, 300µm, and 200µm, respectively, and the alumina specimen used a 610µm nozzle diameter. Line spacing and layer thickness parameters were selected based on a trade-off between efficiency and accuracy for different parts. Radiation distance and heat lamp time have been decided through experimentation; however, these variables are constant for any size of the layer, as only the top surface of the layer is exposed to the heat lamp.

7. Closed-loop Control Using Deep Learning

De La Rosa [17] used a convolutional neural network (CNN) to detect common printing defects and a closed-loop feedback system such that the defects detected would alter the print settings for fused filament fabrication (FFF). Equation 1 describes the process of convolution that the neural network implicitly performs when training. Obtaining fine-tuned values of weights (W) and biases (b) such that the results from inputs (xi) during training matches the results of the control group leads to good neural network performance.

$$f(xi,W) = W\,xi + b \quad (1)$$

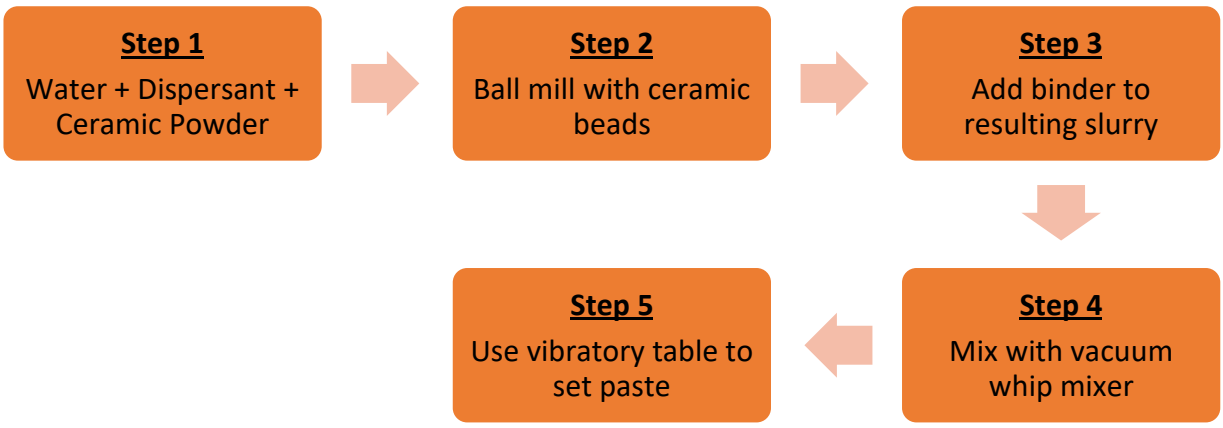

Figure 4. Flowchart for preparing feedstock

Figure 5. Flowchart for postprocessing printed specimens

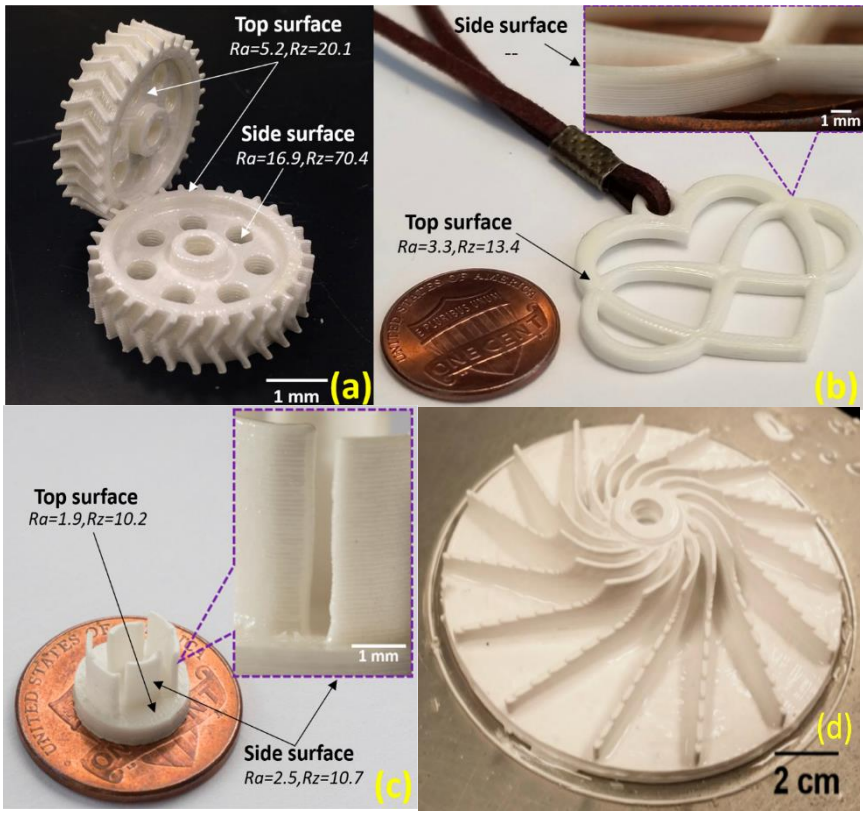

Figure 6. Geometrically complex zirconia (a), (b), (c) and alumina (d) specimens printed using CODE (Images (a), (b), and (c) reproduced from [20], (d) reproduced from [16] with permission from [Elsevier])

A similar method is being implemented to further expand the efficiency and accuracy of the CODE process. De La Rosa [17] used transfer learning from a pre-trained VGG-16 ML model using the Keras library with the Python programming language. Hyperparameters for this model were fine-tuned to work with newly generated data, and the overall image classification testing accuracy achieved was 90%. The dataset used for training the model was generated with a compact USB camera capable of capturing high-resolution images. Images were captured for defects after a random number of printed layers. Since CNNs, in general, require a large dataset for training to be able to predict with high accuracy while avoiding overfitting, dataset expansion, a form of data augmentation, was used by applying transformations to the images such as reshaping, rescaling, rotating, zooming, and altering brightness to already captured images. After applying dataset expansion, the images were then pre-processed by being normalized to be fed into the machine learning (ML) model.

By identifying the defects, the program updates the input G code to modify print parameters such as feed rate, nozzle temperature, material extrusion amount, and fan speed. These updates to the print settings serve as forms of solutions to fix common printing defects in real time. Extrusion-based ceramic 3D printing faces similar problems of common defects. A transfer learning approach to correctly identify defects within the CODE process is being applied. An initial stage of transfer learning would be to obtain a new database of images using a high-resolution camera, labels corresponding to different defects of CODE printing, and a control set of images and labels corresponding to no defects to perform training, validation, and testing. Supervised learning using the initial layer configuration and network hyperparameters is used to perform this process. The images generated could also be subject to data augmentation to increase the number of images for model training and validation. After studying the training dataset and test dataset results using both qualitative and quantitative analyses such

as visual inspection and receiver operating characteristic (ROC) curves, respectively, the results are used to further fine tune and modify the neural network hyperparameters and layer configurations. The ROC curves are plots that are used to determine the frequency at which the CNN predicts the defect correctly and incorrectly. These curves plot the true positive rate on the x-axis and the false positive rate on the y-axis and display the overall prediction accuracy of the network. The true positive and false positive rates are calculated using equations 2 and 3, respectively. The equations inputs include the frequency of true positive, false negative, false positive, and true negative based on the CNN performance.

True Positive Rate = True Positive / (True Positive + False Negative) (2)

False Positive Rate = False Positive / (False Positive + True Negative) (3)

After training the neural network and obtaining a configuration such that the CODE printing defects are detected to a high level of accuracy and precision on the testing dataset, a control system feedback program could be implemented to update printing settings based on the defect detected in real-time. Since the CODE printer uses different hardware and has different printing mechanics than FFF, the program to update the G code would need to account for certain types of defects. CODE does not have certain mechanisms, such as a fan and a heated extruder nozzle, which, when controlled, is used for solutions of common defects in FFF. Instead, CODE uses a heat lamp, an oil bath, and a delay time between printing each layer. Therefore, the printing parameters needed to be updated with G-code are unique. Potential defects for CODE include stringing, over-extrusion, under-extrusion, feedstock agglomeration, depletion of material, feedstock phase separation due to compressed air or material ratios, heat lamp distance, specimen drying time, and level of oil when a specimen is partially submerged. Potential solutions for the previously mentioned common defects for CODE include updating the G code to modify extrusion rate, nozzle travel speed, compressed air flow into the hopper with feedstock, the timing of the heat lamp, distance interval of the vertical axis, delay time between printing each layer. Furthermore, in some situations, the best way to further avoid common defects includes stopping the print. In cases of feedstock agglomeration, depletion of material, or feedstock phase separation, the print needs to be stopped to adjust the feedstock manually.

8. Conclusions

CODE is an extrusion-based 3D printing process for technical ceramics. The feedstock is in the form of a viscous paste. The main materials included in the feedstock are ceramic powder, deionized water, binder, and dispersant. This process has been tested on various technical ceramics, including zirconia and alumina. Parts with varying geometric complexity have been printed using the aforementioned materials. In order to have a completely printed part, there are three major phases: pre-processing, processing, and post-processing. The paste will be prepared during the pre-processing stages and printed during the processing stage. The gradual postprocessing is to ensure that the final ceramic specimens are fabricated without cracks, warpages, or gradients in mechanical properties. A 3D printer was specifically designed, fabricated, and controlled for the CODE process using LinuxCNC as the operating system. The electronics and physical hardware of the printer interface with the host computer using MESA boards which communicate signals through input G code on the LinuxCNC interface. A real-time CNN to detect common printing defects is being applied to the CODE process for defect detection as studied with FFF. Additionally, diverse data augmentation techniques are being applied to increase the overall dataset for the model to aid in defect detection performance. Furthermore, a feedback control program, built on the visual defect detection ML model, is being designed to automatically adjust the printing parameters in real time for implementing potential solutions corresponding with the common defects in the CODE process. This technique will promote overall printing accuracy and efficiency.

Ethical issue

The authors are aware of and comply with best practices in publication ethics, specifically with regard to authorship (avoidance of guest authorship), dual submission, manipulation of figures, competing interests, and compliance with policies on research ethics. The authors adhere to publication requirements that the submitted work is original and has not been published elsewhere.

Data availability statement

Data sharing is not applicable to this article as no datasets were generated or analyzed during the current study.

Conflict of interest

The authors declare no potential conflict of interest.

References

[1] I. Denry and J. Holloway, “Ceramics for dental applications: a review,” Materials, vol. 3, no. 1, pp. 351–368, 2010. [Online]

[2] M. Bohner, L. Galea, and N. Doebelin, “Calcium phosphate bone graft substitutes: failures and hopes,” J. Eur. Ceram. Soc., vol. 32, no. 11, pp. 2663–2671, Aug. 2012. [Online]

[3] F. Kamutzki, S. Schneider, J. Barowski, A. Gurlo, and D. A. H. Hanaor, “Silicate dielectric ceramics for millimetre wave applications,” J. Eur. Ceram. Soc., vol. 41, no. 7, pp. 3879–3894, 2021. [Online]

[4] A. C. Young, O. O. Omatete, M. A. Janney, and P. A. Menchhofer, “Gelcasting of alumina,” J. Am. Ceram. Soc., vol. 74, no. 3, pp. 612–618, Mar. 1991. [Online]

[5] X. Deng, J. Wang, S. Du, F. Li, L. Lu, and H. Zhang, “Fabrication of porous ceramics by direct foaming,” Interceram, vol. 63, pp. 104–108, June. 2014. [Online]

[6] M. H. Bocanegra-Bernal, “Hot isostatic pressing (HIP) technology and its applications to metals and ceramics,” J. Mater. Sci., vol. 39, pp. 6399–6420, Nov. 2004. [Online]

[7] H. Le Ferrand, “Magnetic slip casting for dense and textured ceramics: a review of current achievements and issues,” J. Eur. Ceram. Soc., vol. 41, no. 1, pp. 24–37, Jan. 2021. [Online]

[8] S. M. Olhero, P. M. C. Torres, J. Mesquita-Guimarães, J. Baltazar, J. Pinho-da-Cruz, and S. Gouveia, “Conventional versus additive manufacturing in the structural performance of dense alumina-zirconia ceramics: 20 years of research, challenges and future perspectives,” J. Manuf. Process., vol. 77, pp. 838–879, 2022. [Online]

[9] A. Bove, F. Calignano, M. Galati, and L. Iuliano, "Photopolymerization of ceramic resins by stereolithography process: a review," Appl. Sci., vol. 12, no. 7, p. 3591, Apr. 2022. [Online]
[10] M. A. Saadi, A. Maguire, N. T. Pottackal, M. S. Thakur, M. M. Ikram, A. J. Hart, P. M. Ajayan, and M. M. Rahman, "Direct ink writing: a 3D printing technology for diverse materials," Adv. Mater., vol. 34, no. 28, p. 2108855, Mar. 2022. [Online]
[11] A. Mostafaei, A. M. Elliott, J. E. Barnes, F. Li, W. Tan, C. L. Cramer, P. Nandwana, and M. Chmielus, "Binder jet 3D printing—process parameters, materials, properties, modeling, and challenges," Prog. Mater. Sci., vol. 119, p. 100707, June. 2021. [Online]
[12] N. Kamboj, A. Ressler, and I. Hussainova, "Bioactive ceramic scaffolds for bone tissue engineering by powder bed selective Laser Processing: a review," Materials, vol. 14, no. 18, p. 5338, Sept. 2021. [Online]
[13] N. Travitzky, A. Bonet, B. Dermeik, T. Fey, I. Filbert-Demut, L. Schlier, T. Schlordt, and P. Greil, "Additive manufacturing of ceramic-based materials," Adv. Eng. Mater., vol. 16, no. 6, pp. 729–754, 2014. [Online]
[14] Z. Chen, Z. Li, J. Li, C. Liu, C. Lao, Y. Fu, C. Liu, Y. Li, P. Wang, and Y. He, "3D printing of ceramics: a review," J. Eur. Ceram. Soc., vol. 39, pp. 661–687, 2019. [Online]
[15] A. Zocca, P. Colombo, C. M. Gomes, and J. Günster, "Additive manufacturing of ceramics: issues, potentialities, and opportunities," J. Am. Ceram. Soc., vol. 98, no. 7, pp. 1983–2001, May 2015. [Online]
[16] A. Ghazanfari, W. Li, M. C. Leu, and G. E. Hilmas, "A novel freeform extrusion fabrication process for producing solid ceramic components with uniform layered radiation drying," Addit. Manuf., vol. 15, pp. 102–112, 2017. [Online]
[17] A. D. L. Rosa, "Defect detection and close-loop feedback using machine learning for fused filament fabrication," San Jose State University, San Jose, CA, USA, 2022.
[18] A. Ghazanfari, W. Li, M. Leu, J. Watts, and G. Hilmas, "Mechanical characterization of parts produced by ceramic on-demand extrusion process," Int. J. Appl. Ceram. Technol., vol. 14, no. 3, pp. 486–494, 2017. [Online]
[19] A. Ghazanfari, W. Li, M. C. Leu, J. L. Watts, and G. E. Hilmas, "Additive manufacturing and mechanical characterization of high density fully stabilized zirconia," Ceram. Int., vol. 43, no. 8, pp. 6082–6088, 2017. [Online]
[20] W. Li, A. Ghazanfari, D. McMillen, M. C. Leu, G. E. Hilmas, and J. Watts, "Characterization of zirconia specimens fabricated by ceramic on-demand extrusion," Ceram. Int., vol. 44, no. 11, pp. 12245–12252, 2018. [Online]